Supporting Information

Porous $RuO_xN_yS_z$ Electrodes for Microsupercapacitors and Microbatteries with Enhanced Areal Performances

Sai Gourang Patnaik,† Jensheer Shamsudeen Seenath,† David Bourrier,† Sagar Prabhudev,‡ Daniel Guay,‡ and David Pech*,†

† LAAS-CNRS, Université de Toulouse, CNRS, 7 avenue du colonel Roche, 31400 Toulouse, France.
*E-mail: dpech@laas.fr

‡ INRS-Énergie, Matériaux et Télécommunications, 1650 boulevard Lionel Boulet, Varennes, Québec J3X 1P7, Canada.

Experimental section

1. Elaboration of the electrodes

A Ti(100 nm)/Au(300 nm) thin film was deposited by evaporation on an oxidized silicon substrate and electrochemically pretreated by cycling the potential at a scan rate of 100 mV/s between -0.3 and +1.7 V versus saturated calomel electrode (SCE) in 1 M H_2SO_4 until a stable voltammogram was obtained. Porous metallic current collectors were prepared using the DHBT technique from an optimized solution of 2 x 10^{-3} M of $HAuCl_4.3H_2O$ in 3 M H_2SO_4 by applying 5 A/cm^2 for 20 min in a 3-electrode configuration. The porous Au film was then washed several times in de-ionized water and used as it is as current collector for subsequent deposition of active material. 10 mM of ruthenium nitrosyl sulfate $[Ru(NO)]_2(SO_4)_3$ (Thermofischer Scientific) was dissolved in 100 mL of 0.025 M K_2SO_4 and 0.004 M H_2SO_4. The electrolyte bath was de-aerated with N_2 bubbling for 20 minutes prior to electrodeposition. The solutions were always prepared freshly for deposition and the deposition chamber was kept covered during the entire duration of deposition. The pulse program was optimized to be 10 s of galvanostatic pulse of 7 mA/cm^2 followed by rest period of 30 seconds.

2. Material characterizations

The surface morphology of the electrodes as well as EDX studies were performed by dual beam scanning electron microscope (SEM) on a FEI Helios 600i field emission electron microscope. The surface chemical composition of electrodes were estimated via X-ray photoelectron spectroscopy (XPS) using a VG Escalab 220i-XL instrument operating with a monochromatic

Al Kα X-ray source (1486.6 eV), with exception to powdered nitrosyl sulfate salt that demanded a polychromatic Al Kα source to minimize charging effects.

3. XPS Analysis

The processing of raw spectra acquired involved correction for the non-linear emission background using a Shirley function, subsequently followed by non-linear least-squares curve fitting of the background-subtracted spectra with a series of mixed Gaussian-Lorentzian functions. In certain cases, an asymmetric line-shape of Doniach Sunjic type function was also used, which accounts for any interaction of positive hole created by the photoelectric effect with the conduction electrons. The surface atomic-compositions were estimated using the relation,

$$C_i = \frac{\frac{A_i}{RSF_i}}{\sum \frac{A_i}{RSF_i}}$$

where C_i is the atomic surface concentration of specie i, A_i is the corresponding core-level peak area, and RSF_i the relative sensitivity factor. The surface-compositions were estimated using both Ru-3d and Ru-$3p_{3/2}$ peak area after appropriate elimination of the fitted C-1s core-level contribution. Quantification using both Ru-3d and Ru-$3p_{3/2}$ peak areas led to similar values, and an average was finally used as the reported estimate. Estimation of other elements included use of O-1s, N-1s and S-2p core-level peaks. No other corrections involving peak-shifts were imposed, in other words, the binding energy values reported herein reflect the exact numbers as they were acquired. It is important to note that the individual components in the spectra could not be assigned to any particular chemical state due to unavailability of a suitable reference for recalibration. Specifically, the C-1s edge typically appearing at ~284.8 eV is not obvious in any other sample with exception to RuO_2(001). Neither the N-1s could be treated as a reliable reference without hypothesizing a stable N-1s state in both heat-treated and room-temperature forms.

4. Electrochemical Measurements

The electrochemical synthesis and characterizations were performed with a VMP-3 and a VSP Biologic potentiostat connected to an external 10 A booster channel. For supercapacitors, three electrode set up consisting of Pt mesh as counter electrode, SCE as reference electrode and

porous $RuO_xN_yS_z$ as working electrode was used. LSV studies were performed at 1 mV/s rate at 50°C. All the electrochemical characterizations for supercapacitor studies were performed in 0.5 M H_2SO_4 and doped polyvinyl alcohol (PVA) for interdigitated microsupercapacitors. 1g of PVA was mixed in 10 mL deionized water and heated up to 85°C for 1h under vigorous stirring. Once the polymer is completely dissolved, 1 g H_2SO_4 and 0.2 g SiWa ($H_4SiW_{12}O_{40}$) is added to the mixture and stirred under room temperature. For Li-ion battery studies, the electrodes (0.56 cm^2) were dried to remove any moisture content and tested using Li-ion half-cells (EL-Cell) assembled in a glove box with purified argon, with lithium foil as counter and reference electrodes, and glass fiber separator soaked with 1 M $LiPF_6$ in ethylene carbonate (EC) / diethyl carbonate (DEC) (1:1 volume ratio). For full cell studies, the porous $RuO_xN_yS_z$ electrodes as well as $LiMn_2O_4$ electrodes (Targray) were initially prelithiated w.r.t Li anodes at 0.1C rate. 2 vol % fluroethylene carbonate (FEC) was used as an additive for full cell studies. For long life cycle studies, the cells were initially pre-cycled in the same potential range (0.75 - 3.50 V vs. Li/Li^+) for two cycles at 0.1C (0.1 mA/cm^2) before ramping the rate.

Supplemental Figures

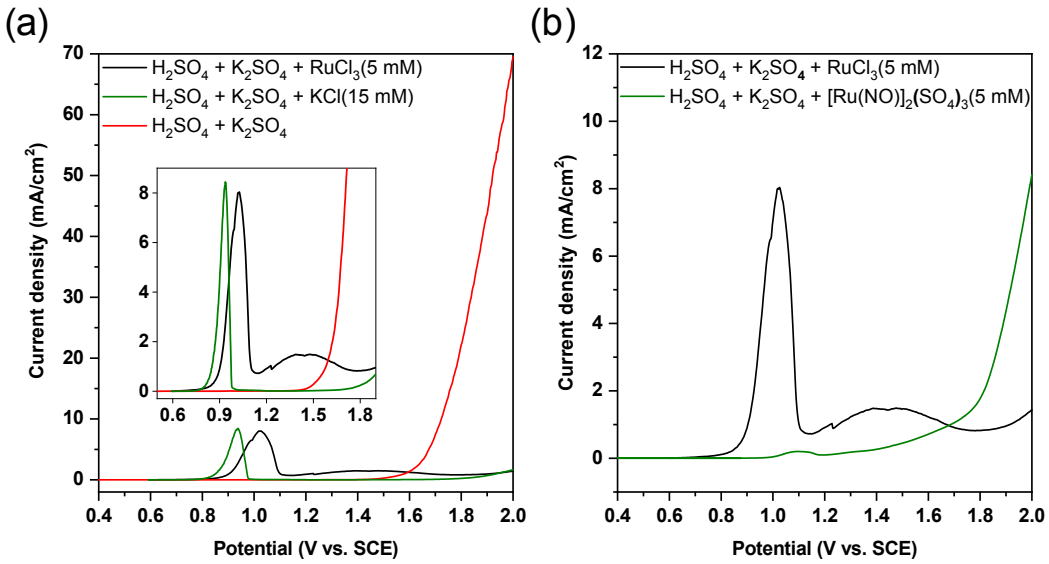

Figure S1. (A) Linear sweep voltammetry (LSV) profiles showing dissolution of porous gold in presence of Cl^- ions. (B) Comparison of LSV profiles with different Ru salts.

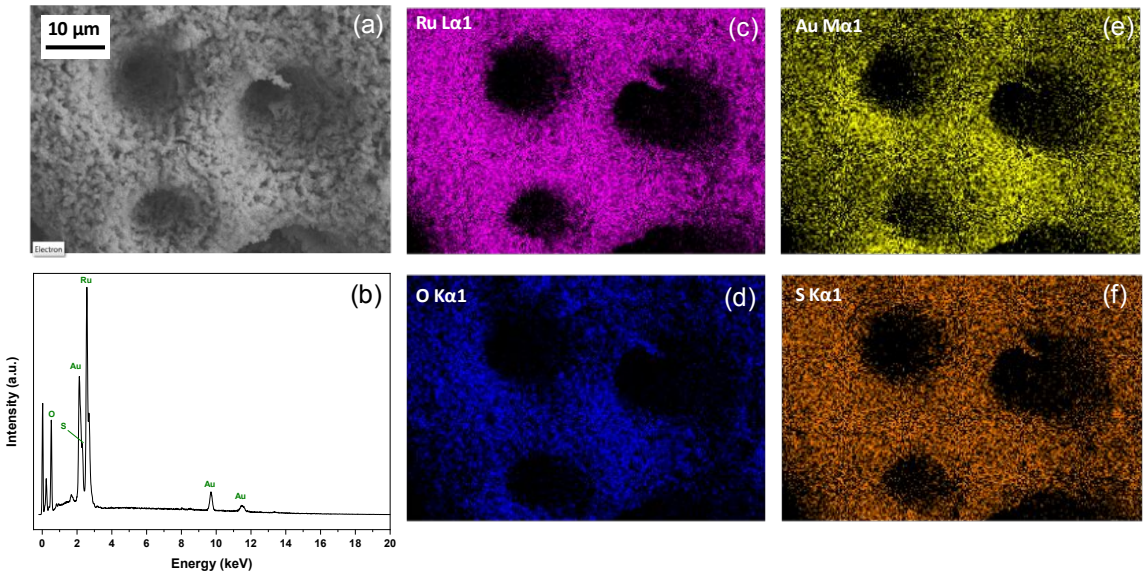

Figure S2. (A) SEM image and (B) EDX spectrum of porous $RuO_xN_yS_z$ after 4 h of deposition. (C), (D), (E) and (F) Elemental mapping showing conformal deposition of Ru species on porous gold surface. Trace contents of other elements including sulfur and oxygen are also observed, which might be oxidative side products from the salt precursor $[Ru(NO)]_2(SO_4)_3]$ utilized for electrodeposition.

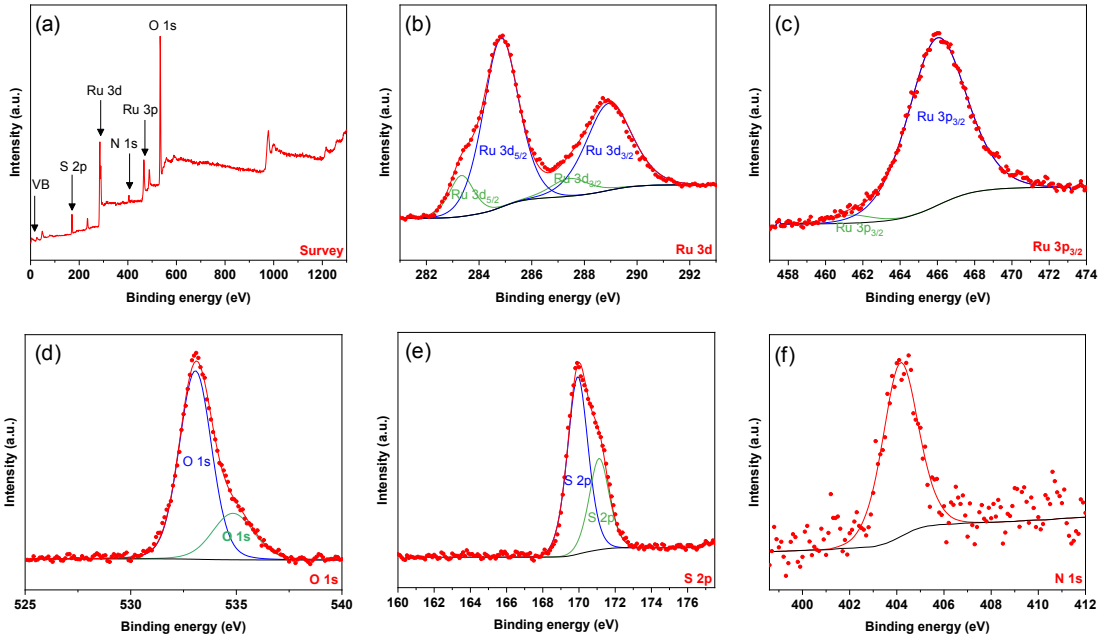

Figure S3. (A) XPS survey and (B), (C), (D), (E) and (F) core-level spectra of the deposited material showing the presence of sulfur and nitrogen.

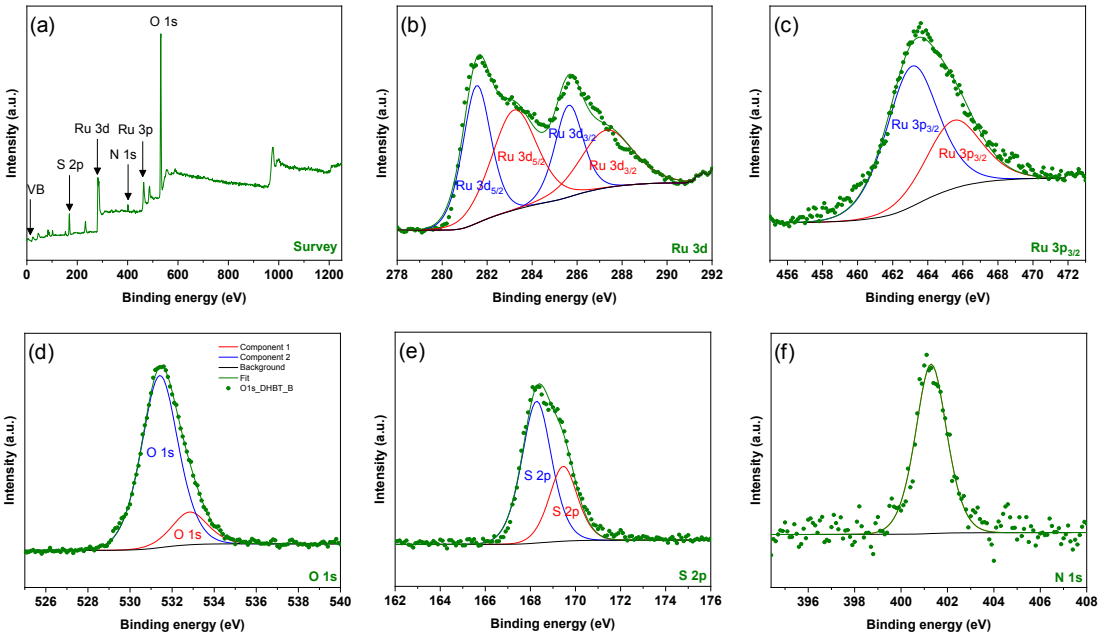

Figure S4. (A) XPS survey and (B), (C), (D), (E) and (F) core-level spectra of the deposited material after heat treatment.

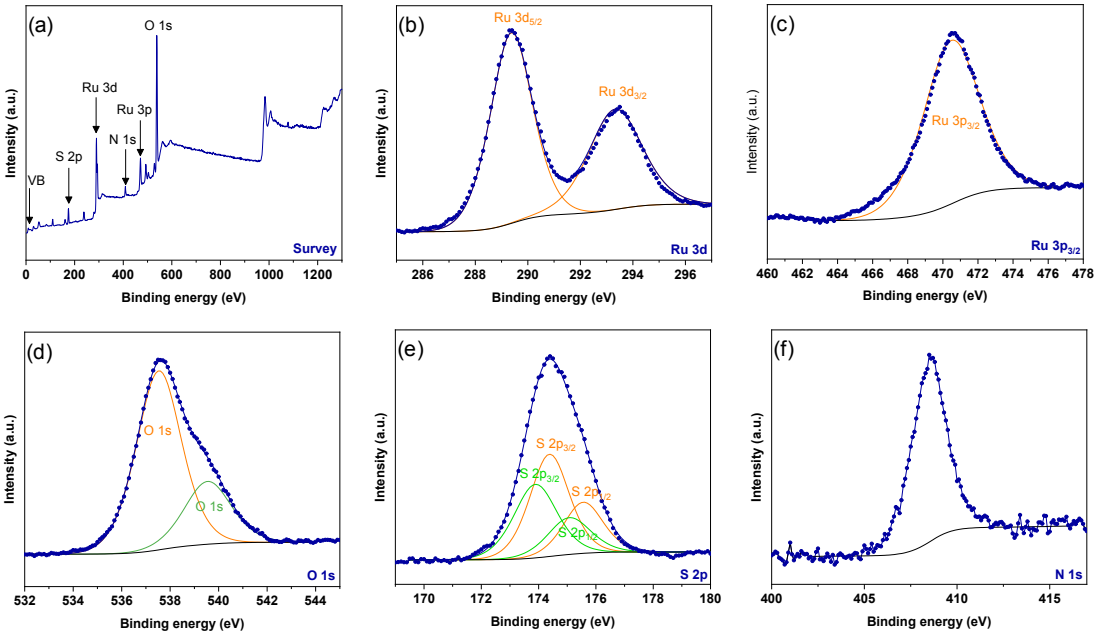

Figure S5. (A) XPS survey and (B), (C), (D), (E) and (F) core-level spectra of the nitrosyl sulfate salt-precursor $[Ru(NO)]_2(SO_4)_3$.

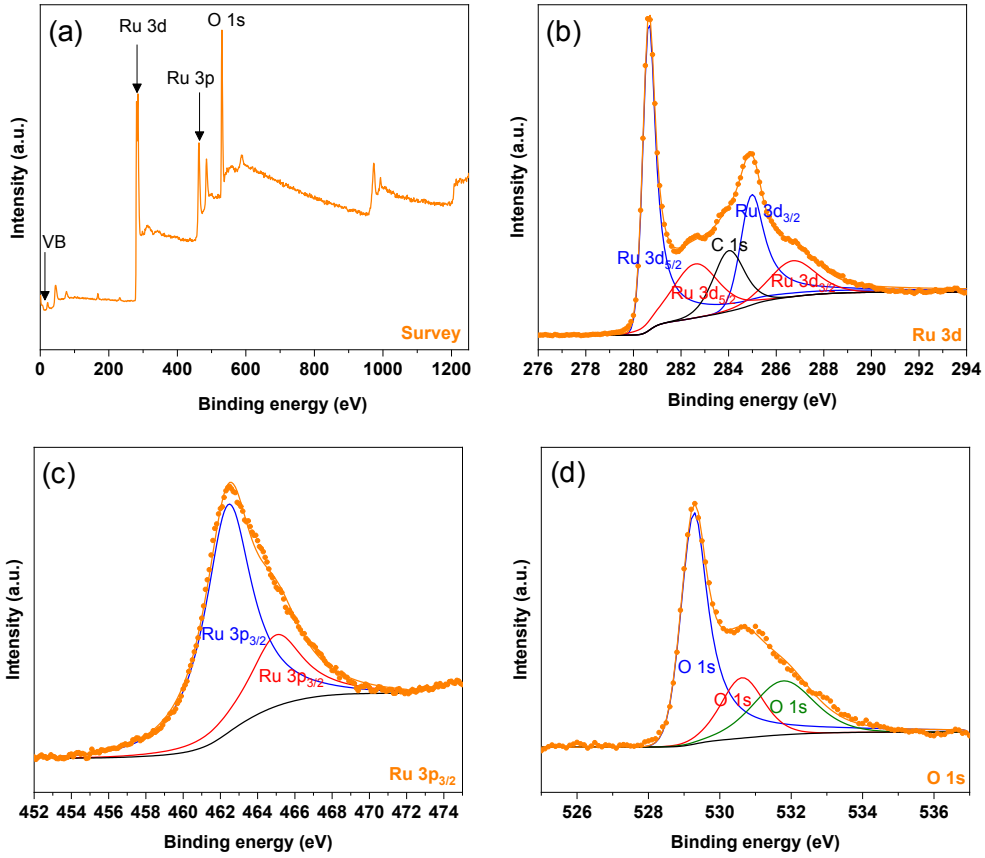

Figure S6. (A) XPS survey and (B), (C) and (D) core-level spectra of a crystalline-RuO_2 reference (RuO_2(001) thin-film synthesized by PLD).

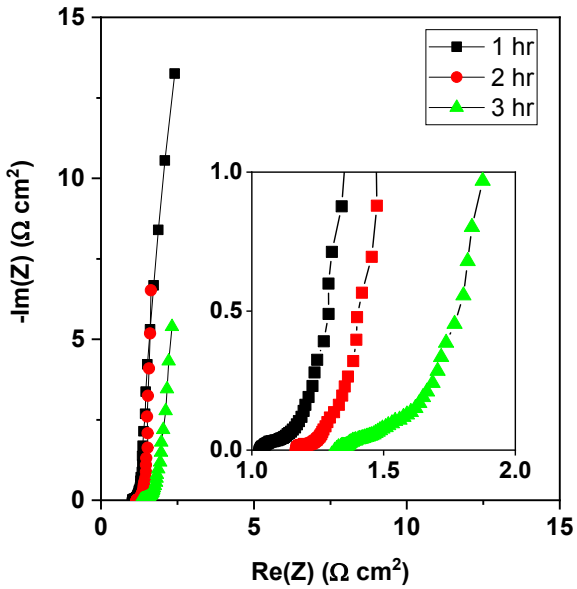

Figure S7. EIS spectrum (100 kHz - 10 mHz) of porous $RuO_xN_yS_z$ synthesized with different durations. No leakage current is observed, with a near-vertical straight line in the low-frequency region typical of a capacitive behaviour. Inset shows the high frequency region.

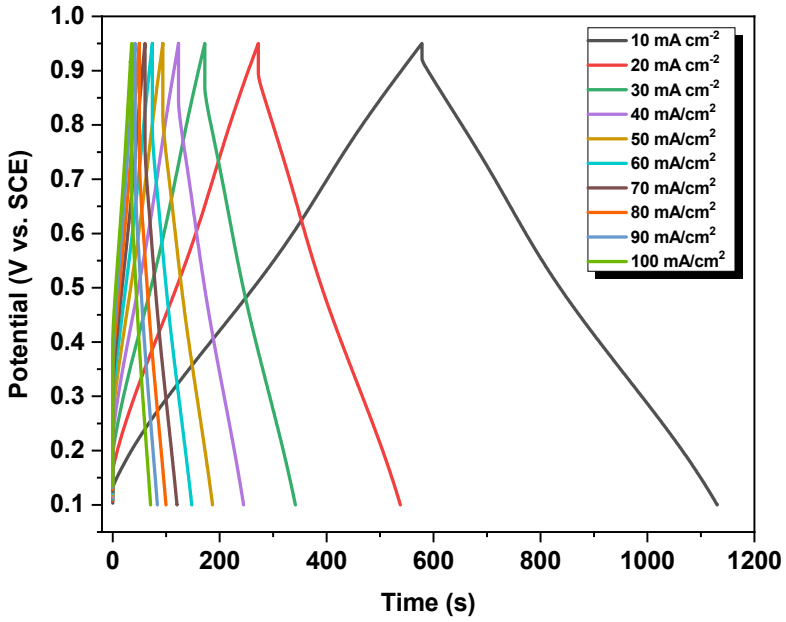

Figure S8. Galvanostatic charge-discharge (GCD) profiles of porous $RuO_xN_yS_z$ (3 hours deposition) at different currents.

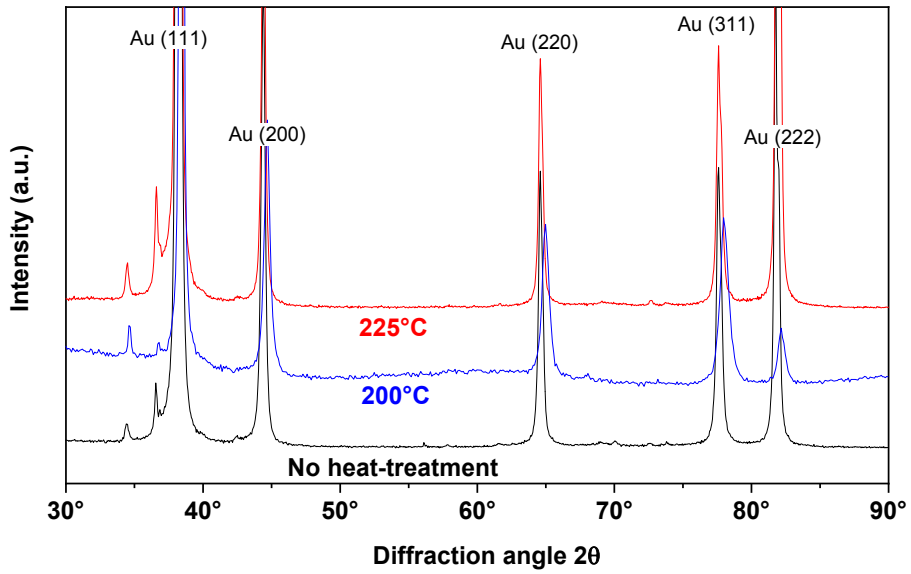

Figure S9. XRD pattern after 1h heat-treatment at 200 and 225°C of $RuO_xN_yS_z$ (1 hour pulse deposition). Only the XRD peaks of the gold substrate are observed.

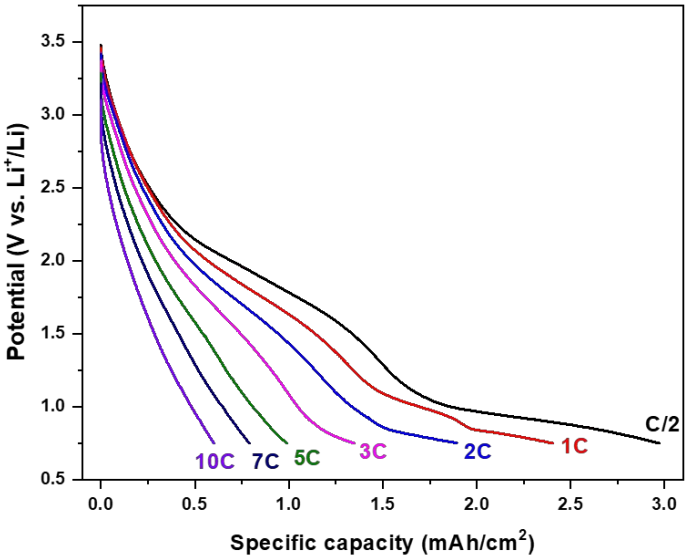

C-rate	Coulombic efficiency
C/2	86.2 %
1C	87.0 %
2C	86.5 %
3C	86.9 %
5C	99.3 %
7C	87.9 %
10C	87.2 %

Figure S10. Charge profiles and coulombic efficiency of porous $RuO_xN_yS_z$ (3 h deposition) as microbattery electrode.

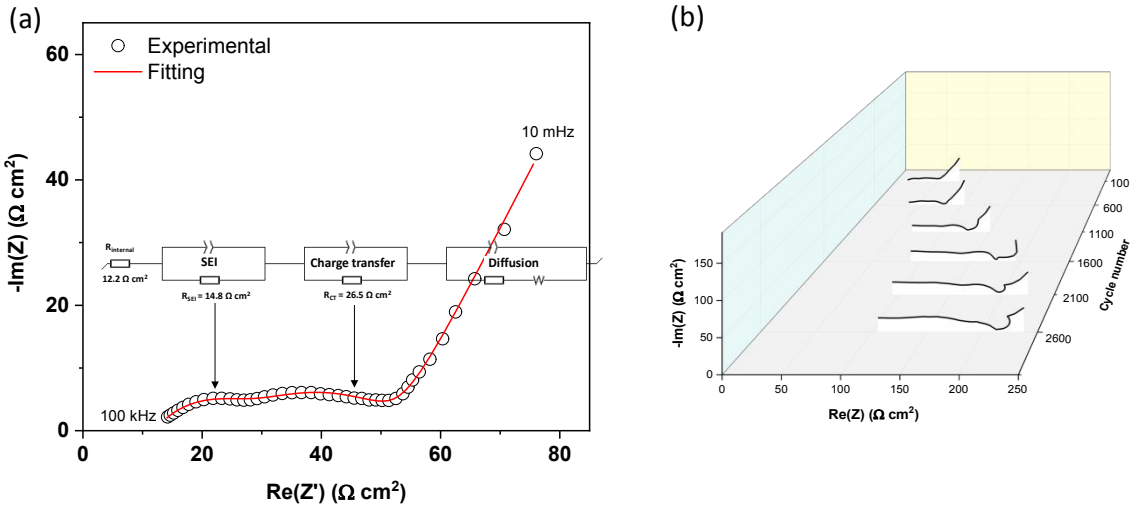

Figure S11. Porous $RuO_xN_yS_z$ electrode (3 h deposition) with Li anode using $LiPF_6$ in EC:DEC. (A) EIS profile (100 kHz - 10 mHz) and corresponding electrical equivalent circuit used to model the system. (B) Evolution of the Nyquist plot with the cycle number.

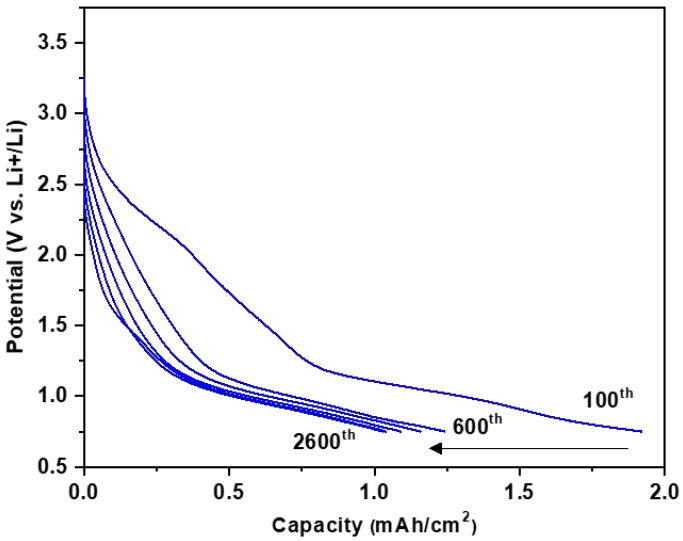

Figure S12. Charge profiles at C/10 rate of porous $RuO_xN_yS_z$ (3 h deposition) as microbattery electrode.

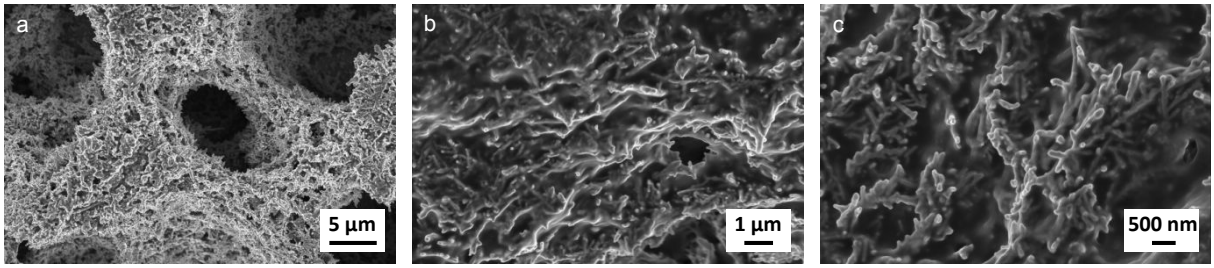

Figure S13. SEM images at different magnifications of the electrode after cycling with Li anode with presence of dendritic network indicating robustness of the Au DHBT structure.

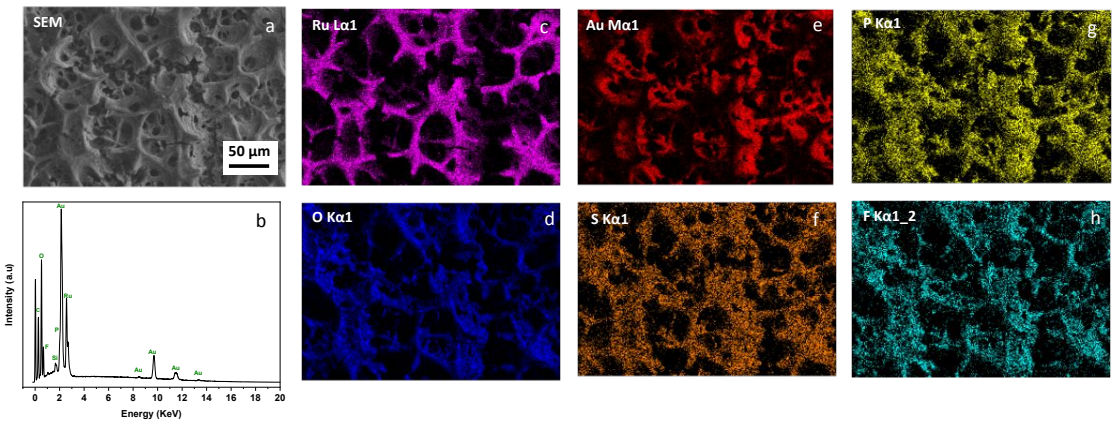

Figure S14. (A) SEM image and (B) EDX spectrum of porous $RuO_xN_yS_z$ after cycling with Li anode. (C), (D), (E), (F), (G) and (H) Elemental mapping showing distribution of different elements including SEI formation.

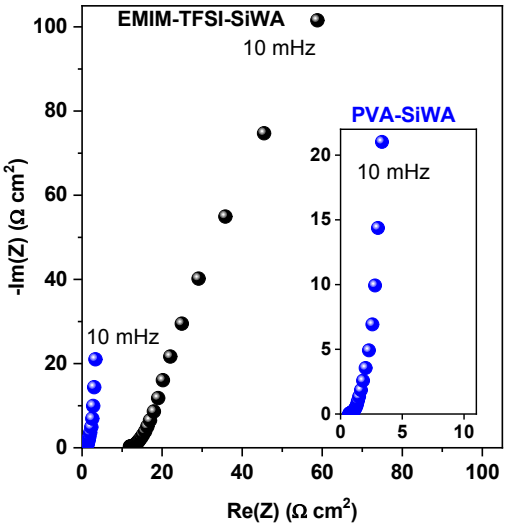

Figure S15. Nyquist plot of the interdigitated $RuO_xN_yS_z$ microsupercapacitors based on doped PVA and doped EMIM-TFSI. Inset shows a zoom view.